

Modeling Non-Uniform Hypergraphs Using Determinantal Point Processes

Yichao Chen*

Department of Statistics, University of Michigan, Ann Arbor, Michigan

Jingfei Zhang†

Goizueta Business School, Emory University, Atlanta, Georgia

Ji Zhu‡

Department of Statistics, University of Michigan, Ann Arbor, Michigan

Abstract

Most statistical models for networks focus on pairwise interactions between nodes. However, many real-world networks involve higher-order interactions among multiple nodes, such as co-authors collaborating on a paper. Hypergraphs provide a natural representation for these networks, with each hyperedge representing a set of nodes. The majority of existing hypergraph models assume uniform hyperedges (i.e., edges of the same size) or rely on diversity among nodes. In this work, we propose a new hypergraph model based on non-symmetric determinantal point processes. The proposed model naturally accommodates non-uniform hyperedges, has tractable probability mass functions, and accounts for both node similarity and diversity in hyperedges. For model estimation, we maximize the likelihood function under constraints using a computationally efficient projected adaptive gradient descent algorithm. We establish the consistency and asymptotic normality of the estimator. Simulation studies confirm the efficacy of the proposed model, and its utility is further demonstrated through edge predictions on several real-world datasets.

Keywords: hypergraphs; higher-order interactions; determinantal point process; nonuniform hyperedges; constrained estimation.

*Email: yichaoc@umich.edu

†Email: emma.zhang@emory.edu

‡Email: jizhu@umich.edu

1 Introduction

Existing network analyses have primarily focused on pairwise interactions, where each edge in the network consists of two nodes. However, higher-order interactions, which involve multiple nodes simultaneously, are ubiquitous across many real-world scenarios. For example, in academic collaborations, researchers often co-author papers in teams of three or more. In protein-protein or gene-gene interactions, multiple proteins or genes may work as a group to carry out biological functions. Existing studies have demonstrated the importance of higher-order interactions in contexts such as neural systems (Yu et al., 2011), genetic networks (Ritz et al., 2014), and the spread of epidemics (Battiston et al., 2021). Despite their importance, these high-order interactions are often simplified into pairwise interactions in existing analyses (Grover and Leskovec, 2016; Cao et al., 2015), resulting in substantial information loss. For example, in co-author networks, a paper co-authored by three or more represents a collaborative effort among all co-authors. Reducing this high-order interaction to pairwise connections fails to capture the full information of the collaboration. A more natural approach is to directly model higher-order interactions, allowing for richer and more accurate representations of complex systems.

High-order interactions among a set of nodes can be naturally represented using *hypergraphs*, a generalization of traditional graphs where an edge, known as a *hyperedge*, is a set that includes all interacting nodes. For example, in a co-author network, nodes represent authors and a hyperedge corresponds to the set of authors of a paper. Recent studies have explored hypergraphs through various approaches. One line of work transforms hypergraphs into weighted graphs using hypergraph Laplacians (Ghoshdastidar and Dukkipati, 2017a; Chien et al., 2018), where edge weights are based on the counts of hyperedges shared by each node pair. Other works focus on simplicial hypergraphs, which require that the presence of a hyperedge implies the presence of all its subsets (Lunagómez et al., 2017; Bobrowski and Kahle, 2018). Another line investigates uniform hypergraphs, where all hyperedges contain the same number of nodes (Ghoshdastidar and Dukkipati, 2017b; Ke et al., 2019; Yuan and Qu, 2022; Lyu et al., 2023). Extensions to non-uniform hypergraphs have been proposed by either augmenting hyperedges with null vertices to create uniform multi-hypergraphs (Zhen and Wang, 2023) or by combining multiple uniform hypergraphs of different orders (Yuan et al., 2022; Turnbull et al., 2023; Nandy and Bhattacharya, 2024). The majority of these works focus on network community detection and represented hypergraphs using tensors. However, tensor-based representations can be computationally inefficient, as the order of the tensor is determined by the hyperedge with the largest cardinality, leading to significant scalability challenges. They also cannot accommodate multi-hyperedges. That is, two or more hyperedges connecting the same set of nodes, which can occur, for example, when one group of co-authors collaborated on several papers. Notably, Yu and Zhu (2025) proposed a flexible non-uniform latent space hypergraph model that accounts for

multi-hyperedges. Their model naturally accommodates non-uniform hyperedges and has a tractable probability mass function. In particular, their model is defined via a class of determinantal point process, a discrete probabilistic model parameterized by a kernel matrix. The proposed model assigns a probability to every subset of nodes based on the diversity of the included nodes, and nodes with diverse latent positions are more likely to form hyperedges. While assuming diversity can be plausible in some settings, such as ingredients in a recipe, similarity, where similar nodes may more likely to appear in an hyperedge, can be more plausible in many other settings, such as co-authors on a paper.

In our work, we propose a new hypergraph model using a more flexible class of determinantal point processes. The proposed model naturally accommodates non-uniform hyperedges, has tractable probability mass functions, and allows for node similarity or diversity in hyperedges. In particular, we consider a nonsymmetric kernel matrix, which overcomes the restrictive negative association property induced by symmetric kernels (Brunel, 2018) and represents a major improvement over Yu and Zhu (2025). For model estimation, we maximize the likelihood function under constraints via a computationally efficient projected adaptive gradient descent algorithm. For theoretical results, we show the consistency and the asymptotic normality for the constrained maximum likelihood estimators. The special manifold of the parameter space of our model leads to a challenging proof, especially for the asymptotic normality. Notably, the asymptotic distribution is intricately linked to a tangent cone with a unique structure. The nonsymmetric kernel matrix in our model results in a unique tangent cone, requiring very delicate derivations to derive asymptotic normality.

2 Model

2.1 Notation

Write $[k] = \{1, 2, \dots, k\}$. Let $\|\cdot\|_2$ denote the vector ℓ_2 -norm, $\|\cdot\|_F$ the matrix Frobenius norm and $\det(\cdot)$ the determinant of a matrix. Denote the i th row and j th column of a matrix M as $M_{i \cdot}$ and $M_{\cdot j}$, respectively. Let $\text{vec}(M)$ denote the vector formed by concatenating the columns of matrix M , and $\text{diag}(M)$ denote the vector with diagonals of matrix M . Let $\text{vec}^{-1}(\cdot)$ be the inverse function of $\text{vec}(\cdot)$ such that $\text{vec}^{-1}(\text{vec}(M)) = M$. Write H_n as the set of $n \times n$ diagonal matrix with diagonal elements in $\{-1, 1\}$, and O_d as the set of $d \times d$ orthogonal matrices. Given a $n \times n$ matrix M , denote M_{e_s} as the $|e_s| \times |e_s|$ principal submatrix of M indexed by $e_s \subset [n]$.

2.2 Determinantal Point Process

A point process on a set V is a probability measure defined over finite subsets of V . In the case of discrete, finite point processes, where $V = \{1, 2, \dots, n\}$, a point process on V is a probability measure

over all subsets of V . A point process on V is called a *determinantal point process* if, for a randomly drawn subset $E \subseteq V$ and a given subset $e \subseteq V$, the following probability equation holds for an $n \times n$ matrix L :

$$pr_L(E = e) \propto \det(L_e).$$

By the property of matrix determinant, it can be shown that $\sum_{e \subseteq V} \det(L_e) = \det(L + I)$, where I is the identity matrix. Correspondingly, the following holds

$$pr_L(E = e) = \frac{\det(L_e)}{\det(L + I)}. \quad (1)$$

The matrix L is referred to as a *kernel matrix*. Not all matrices L are admissible to define a determinantal point process. A matrix L is admissible if and only if all principal minors of L are nonnegative (Brunel, 2018); such matrices are called P_0 -matrices.

The majority of existing literature on determinantal point processes assume L to be symmetric and positive semidefinite (Kulesza et al., 2012; Lavancier et al., 2015; Kang, 2013), which is a special case of P_0 -matrices. Interestingly, assuming symmetry on L induces a strong property of negative dependence called *negative association* (Brunel, 2018). To explain this property, we first introduce the marginal kernel matrix K , where $K = I - (L + I)^{-1}$. For a given subset $e \subseteq V$ and a randomly drawn subset $E \subseteq V$, it holds under (1) that

$$pr(e \subseteq E) = \det(K_e).$$

It is seen that K models the marginal probabilities of subsets. If $e = \{i\}$, then $pr(i \in E) = K_{ii}$. When L is symmetric, K is also symmetric. Under symmetric kernels one can show that $\text{Cov}\{1(i \in E), 1(j \in E)\} = -K_{ij}^2$ for any $i \neq j$. More generally, for any two disjoint sets $e_1, e_2 \in V$, it holds that $\text{Cov}\{1(e_1 \subseteq E), 1(e_2 \subseteq E)\} = \det(K_{e_1 \cup e_2}) - \det(K_{e_1}) \det(K_{e_2}) \leq 0$ (Borcea et al., 2009). This negative association from symmetric kernels forces repulsive interactions between items in V .

2.3 A New Non-uniform Hypergraph Model

Let $V = [n]$ denote the set of n nodes, and $D = \{e_1, e_2, \dots, e_m\}$ the set of m observed hyperedges. Each hyperedge can be represented as a subset of V , that is, $e_s \subseteq [n]$ for $s \in [m]$. We assume that e_s for $s \in [m]$ follows

$$e_s \stackrel{\text{i.i.d.}}{\sim} pr_L,$$

where L is a kernel matrix and pr_L is as defined as (1). Modeling hyperedges using determinantal point processes has several benefits. First, it naturally accommodates non-uniform hyperedges and

multi-hyperedges, which greatly extends model flexibility. Second, as the normalizing constant can be easily derived, pr_L defines a tractable distribution over all possible hyperedges, facilitating estimation, inference, and sampling. Third, the kernel matrices L and K enhance model interpretability as discussed in Section 2.2.

To introduce more flexibility when forming hyperedges, we consider a general form of kernel matrices that are not necessarily symmetric. Since the kernel matrix L needs to be a P_0 -matrix, we choose L such that $L+L^T$ is a positive semidefinite matrix, which is a sufficient condition for L to be a P_0 -matrix. We propose the following nonsymmetric determinantal point process hypergraph model:

$$pr_L(E = e) = \frac{\det(L_e)}{\det(L + I)}, \quad (2)$$

$$L = BVV^T B + \gamma \cdot BVCV^T B + B^2,$$

where B is a $n \times n$ diagonal matrix whose diagonal elements β_i 's are non-negative and characterize node popularity. The matrix V is a $n \times d$ with the constraint $\|v_i\|_2 = 1$, where v_i denotes the i th row of V . The vector v_i can be viewed as the latent space position for the i th node (See Equation 4). The matrix C is a skew matrix satisfying $C^T = -C$, with the constraint that $\|C\|_F = 1$. This special form of C is chosen to guarantee that $L + L^T$ is a positive semidefinite matrix. The scalar $\gamma \geq 0$ is a scaling parameter for the skew matrix C . The extra term B^2 is introduced to ensure L is full-rank. If L is rank-deficient, then $pr_L(E = e) = 0$ for $|e| > \text{rank}(L)$, as $\det(L_e) = 0$. We write the hypergraph model in (2) as $H(L)$ or $H(B, V, C, \gamma)$.

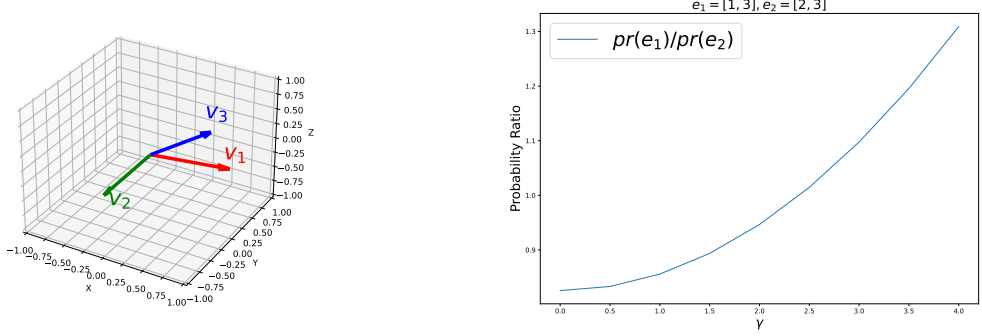
To help understanding (2), we consider a two-element set $\{i, j\}$, which gives:

$$pr_L(E = \{i, j\}) \propto 4\beta_i^2\beta_j^2 - \beta_i^2\beta_j^2 \cos^2(v_i, v_j) + \gamma^2\beta_i^2\beta_j^2(v_i^T C v_j)^2. \quad (3)$$

When β_i 's are fixed and $\gamma = 0$, the probability $pr_L(E = \{i, j\})$ is driven by $-\cos^2(v_i, v_j)$. Correspondingly, this model encourages diversity, that is, nodes with unaligned latent positions are more likely to form hyperedges. When $\gamma \neq 0$, the term $(v_i^T C v_j)^2$ may encourage nodes with similar latent positions to form hyperedges. For example, set $d = 3$ and consider C in the form of

$$C = \begin{bmatrix} 0 & \lambda_3 & -\lambda_2 \\ -\lambda_3 & 0 & \lambda_1 \\ \lambda_2 & -\lambda_1 & 0 \end{bmatrix},$$

where $\lambda_1, \lambda_2, \lambda_3 \in R$. The matrix C is determined by the vector $\lambda = (\lambda_1, \lambda_2, \lambda_3)$. By properties of skew-symmetric matrices, we have $v_i^T C = (\lambda \times v_i)^T$ where $\lambda \times v_i$ represents the cross product between



(a) Latent positions for v_1, v_2, v_3

(b) The changes of probability ratio as γ changes

Figure 1: An illustration of the non-symmetric determinantal point process hypergraph model.

λ and v_i . That is, we have

$$P(E = \{i, j\}) \propto 4\beta_i^2\beta_j^2 - \beta_i^2\beta_j^2 \cos^2(v_i, v_j) + \gamma^2\beta_i^2\beta_j^2 \cos^2(\lambda \times v_i, v_j). \quad (4)$$

The direction of vector $\lambda \times v_i$ is perpendicular to both λ and v_i , and the magnitude of vector $\lambda \times v_i$ is the area of the parallelogram spanned by λ and v_i . The cross product $\lambda \times v_i$ leads to the position change for a node latent vector v_i and two diverse nodes may form hyperedges with smaller probabilities. In addition, as we increase the value of γ , the term $\gamma^2\beta_i^2\beta_j^2 \cos^2(\lambda \times v_i, v_j)$ contributes more to the probability. In summary, v_i 's, γ and λ together modulate the probabilities of forming hyperedges.

In Figure 1, we present an illustrative example with latent positions vectors v_1, v_2, v_3 and the probabilities of $e_1 = \{1, 3\}$ and $e_2 = \{2, 3\}$ with varying values of γ . Since the latent positions v_1 and v_3 are more similar than v_2 and v_3 , we have $pr(e_1)/pr(e_2) < 1$ when $\gamma = 0$, corresponding to a symmetric kernel and encourages diversity in the generated hyperedges. As γ increases, the ratio of $pr(e_1)/pr(e_2)$ increases monotonically. When $pr(e_1)/pr(e_2) > 1$, similar positions v_1 and v_3 are more likely to form hyperedges compared to diverse positions v_1 and v_2 . This example demonstrates the extra flexibility provided by the non-symmetric kernel matrix L in our model.

2.4 Model Properties and Sampling

Based on model (2), we can derive the following useful properties on the marginal and conditional distributions.

Marginal Distribution. Recall $K = I - (L + I)^{-1}$. Under (2), the marginal probability for node i

to be included in a random hyperedge is

$$pr(i \in E) = K_{ii}.$$

Conditional Distribution. For any $e_1 \subset e_2 \subset [n]$ and under (2), we have

$$pr(E = e_2 \mid e_1 \subset E) = \frac{\det(L_{e_2})}{\det(L + I - I_{e_1})} \quad (5)$$

where I_{e_1} is a $n \times n$ diagonal matrix with $\{I_{e_1}\}_{ii} = 1$ if $i \in e_1$, and $\{I_{e_1}\}_{ii} = 0$ otherwise.

Invariant to node ordering. Under (2), the probability of forming a hyperedge e is invariant to the ordering of nodes in the hyperedge e and the node set V . This follows from the determinant's properties. Any reordering of nodes can be achieved through a sequence of pairwise swaps. Swapping two nodes requires swapping two rows and two columns in the corresponding kernel matrix. According to Section 5.3 of [Hoffmann and Kunze \(1971\)](#), each such swap affects only the sign of the determinant without altering its absolute value. Consequently, swapping two nodes does not change the values of $\det(L_e)$ and $\det(L + I)$, ensuring that the probability of forming hyperedges remains invariant to node ordering.

Given model parameters B, V, C, γ , hyperedges can be directly sampled from (2) using the following algorithm

```

Set  $Z = (B^2 + I)^{-1}BV$ ,  $W = ((I_d + \gamma C)^{-1} + V^T B (B^2 + I_n)^{-1} BV)^{-1}$ ,  $Y = \emptyset$ ;
for  $i = 1$  to  $n$  do
     $p_i \leftarrow z_i^T W z_i$ ;
     $u \leftarrow \text{uniform}(0, 1)$ ;
    if  $u \leq p_i$ , then  $Y \leftarrow Y \cup \{i\}$ ; else  $p_i \leftarrow p_i - 1$  ;
     $W \leftarrow W - \frac{W z_i z_i^T W}{p_i}$ ;
return  $Y$ 

```

Algorithm 1: Hyperedge Sampling from (2)

Algorithm 1 is adapted from Theorem 2 in [Poulson \(2020\)](#), which provides a factorization-based sampling method for generic determinantal point processes. To sample a hyperedge, we initialize it as an empty set and iterate through each node to decide if it should be included based on decisions for previous nodes. The inclusion/exclusion decisions need to be made with the appropriate conditional probabilities, which can be calculated based on the properties of model (2).

2.5 Identifiability

For model (2), it can be shown that the matrix V is identifiable up to an orthogonal transformation and sign flips for rows, and the matrix C is identifiable up to orthogonal transformation on both sides.

The formal results are presented in Theorem 1, and its proof is collected in the supplement.

Theorem 1 Suppose $S \in H_n$, $O \in O_d$ and matrix V is full rank. For two different kernel matrices $L_1 = B_1 V_1 V_1^T B_1 + \gamma_1 B_1 V_1 C_1 V_1^T B_1 + B_1^2$ and $L_2 = B_2 V_2 V_2^T B_2 + \gamma_2 B_2 V_2 C_2 V_2^T B_2 + B_2^2$, L_1 and L_2 give equivalent hypergraph models if $L_1 = S L_2 S$. Furthermore, we have $L_1 = S L_2 S$ if and only if $V_1 = S V_2 O^T$, $C_1 = O C_2 O^T$, $B_1 = B_2$ and $\gamma_1 = \gamma_2$.

2.6 Parameter Estimation

Given an observed set of hyperedges $D = \{e_1, \dots, e_m\}$, we aim to estimate parameters B, V, C, γ . Under (2), the likelihood function can be written as

$$\begin{aligned} \phi(B, V, C, \gamma) = \\ \frac{1}{m} \sum_{s=1}^m \log \det (B_{e_s} V_{e_s} (I + \gamma C) V_{e_s}^T B_{e_s} + B_{e_s}^2) - \log \det (B V (I + \gamma C) V^T B + B^2 + I). \end{aligned}$$

We consider the following constrained optimization problem:

$$\begin{aligned} \max_{B, V, C, \gamma} \quad & \phi(B, V, C, \gamma) \\ \text{s.t.} \quad & \text{diag}(B) > 0, \quad \text{diag}(V V^T) = 1, \quad \|C\|_F = 1. \end{aligned}$$

This objective function is nonconvex, and we propose to solve it via an efficient projected adaptive gradient descent algorithm. The detailed algorithm is provided in the supplement. The adaptive gradient descent algorithm was first proposed in (Kingma and Ba, 2014), and is usually referred to as the Adam algorithm. The learning rate is adaptively chosen and gradually reduced until the loss has stopped improving. The Adam algorithm combines desirable features of Momentum (Qian, 1999) and RMSprop (Tieleman and Hinton, 2012). Compared with a standard project gradient descent, it can provide adaptive learning rates, faster convergence, and robustness to the choice of hyperparameters. It has been proven to work well in many non-convex optimization problems. When implementing this algorithm, multiple random initial values are chosen and we select the results with the maximum objective value. We use the cross-validation approach to select d in real-world data analysis.

3 Theoretical results

This section establishes the consistency and asymptotic normality of the MLE estimates. We first introduce some notation. Define the parameter space for $\omega = (V, B, C, \gamma)$ as

$$\Omega = \{V \in R^{n \times d}, B \in R^{n \times n}, C \in R^{d \times d}, \gamma \in R \mid \|v_i\|_2 = 1 \text{ for all } i, \\ \|C\|_F = 1, B \text{ is diagonal with } \text{diag}(B) > 0, 0 \leq \gamma \leq T\},$$

where T is a finite scalar. Define function $\Upsilon : \Omega \rightarrow R^{n \times n}$ as $\Upsilon(\omega) = BVV^T B + \gamma BVCV^T B + B^2$. Correspondingly, the parameter space for L is $\Psi = \{\Upsilon(\omega) \mid \omega \in \Omega\}$. Let $\bar{\Psi}$ be the closure of Ψ . Denote the true model parameters as $\omega^* = (V^*, B^*, C^*, \gamma^*)$ and the true kernel matrix as L^* , where $L^* = \Upsilon(\omega^*)$. The Jacobian matrix of $\Upsilon(\omega)$ at ω^* is denoted as $\nabla \Upsilon(\omega^*)$.

We rewrite the log-likelihood as a function of L such that

$$\phi(L) = \sum_{e \subseteq [n]} \hat{p}_e \log \det(L_e) - \log \det(L + I),$$

where $\hat{p}_e = \frac{1}{m} \sum_{s=1}^m I(e_s = e)$. Define $p_e(L) = \frac{\det(L_e)}{\det(L + I)}$, and we have

$$\begin{aligned} \Phi(L) &= E(\phi(L)) = \sum_{e \subseteq [n]} p_e(L^*) \log \det(L_e) - \log \det(L + I) \\ &= \sum_{e \subseteq [n]} p_e(L^*) \log \frac{\det(L_e)}{\det(L + I)}, \end{aligned} \tag{6}$$

where the second equality holds true since $\sum_{e \subseteq [n]} p_e(L^*) = 1$. The theorem below shows consistency of the MLE estimates.

Theorem 2 *Given an observed hypergraph on n nodes with m hyperedges independently generated from (2), we consider the MLE estimates $\hat{B}, \hat{V}, \hat{C}, \hat{\gamma}$ for the unknown true parameters B^*, V^*, C^*, γ^* with $(B^*, V^*, C^*, \gamma^*) \in \Omega$. Let $\delta = \min_{e \subseteq [n]} p_e(L^*)$. Assuming V^* is a full-rank matrix and $2^{n+1}e^{-\delta^2 m/2} \rightarrow 0$, we have, as $m \rightarrow \infty$,*

$$\begin{aligned} \min_{\{S \in H_n, O \in O_d\}} \|S\hat{V}O^T - V^*\|_F &\xrightarrow{p} 0, \quad \min_{\{O \in O_d\}} \|O\hat{C}O^T - C^*\|_F \xrightarrow{p} 0, \\ \|\hat{B} - B^*\|_F &\xrightarrow{p} 0, \quad \|\hat{\gamma} - \gamma^*\|_F \xrightarrow{p} 0, \quad \min_{\{S \in H_n\}} \|S\hat{L}S - L^*\|_F \xrightarrow{p} 0. \end{aligned}$$

The detailed proof is collected in the supplement. The proof utilizes Theorem 5.14 in [Van der Vaart \(2000\)](#) and follows a similar strategy as in [Yu and Zhu \(2025\)](#). Theorem 5.14 in [Van der Vaart \(2000\)](#) shows that under some regularity conditions and for every compact set in the parameter space, the

MLE estimator belonging to that compact set converges to the true parameter when the number of samples goes to infinity. It is a fundamental result for establishing the consistency of MLE estimators. One key step in the proof is to construct a compact set based on our parameter space that almost surely contains the estimators. Unlike [Yu and Zhu \(2025\)](#), which assumes the number of nodes n is fixed, our result in [Theorem 2](#) allows n to diverge as long as $2^{n+1}e^{-\delta^2 m/2} \rightarrow 0$. By the definition of δ , this can be seen as a sparsity condition.

Before we establish the asymptotic normality of the MLE estimates, some more definitions are in order.

Definition 1: (Matrix Irreducibility). A given matrix $M_{n \times n}$ is reducible if there exists a partition $\{J_1, J_2, \dots, J_K\}$ of $[n]$ with $K > 1$, such that $M_{ii'} = 0$ whenever $i \in J_k, i' \in J_{k'}$ and $k \neq k'$. Otherwise, the matrix M is said to be irreducible.

Definition 2: (Bouligand tangent cone). The Bouligand tangent cone of a set $C \in \mathbb{R}^d$ at the point $x \in C$ is the set defined as

$$T_C(x) = \left\{ v \in \mathbb{R}^d \mid \exists \{x_n\} \in C, \{\tau_n\} \in \mathbb{R}^+, x_n \rightarrow x, \tau_n \rightarrow 0, \frac{x_n - x}{\tau_n} \rightarrow v \right\}.$$

A vector v lies in the Bouligand tangent cone of C if and only if there exist a sequence $\tau_n \rightarrow 0$ and a sequence $x_n \rightarrow x$ in C such that $(x_n - x) / \tau_n \rightarrow v$. See [Geyer \(1994\)](#) for more details.

With a slight abuse of notation, we define $\text{vec}(\bar{\Psi}) = \{\text{vec}(M) \mid M \in \bar{\Psi}\}$, and use $T_{\text{vec}(\bar{\Psi})}(\text{vec}(L^*))$ to denote the Bouligand tangent cone of $\text{vec}(\bar{\Psi})$ at $\text{vec}(L^*)$.

Theorem 3 *Given an observed hypergraph on n nodes with m hyperedges independently generated from (2) with the true kernel matrix L^* . Consider the maximum likelihood estimate \hat{L} of L^* , and let*

$$\tilde{L} = \arg \min_{M \in \{S\hat{L}S \mid S \in H_n\}} \|M - L^*\|_F.$$

If V is full rank and irreducible, then as $m \rightarrow \infty$ while n remains fixed, we have

$$\sqrt{m} \cdot \text{vec}(\tilde{L} - L^*) \xrightarrow{\text{dist}} N\left(0, Q \left(Q^T \nabla^2 F(\xi^*) Q\right)^{-1} Q^T\right) \text{ as } m \rightarrow \infty,$$

where $\xi^ = \text{vec}(L^*)$, $F(\xi) = -\Phi(\text{vec}^{-1}(\xi))$, and Q is an orthogonal matrix (i.e. $Q^T Q = I$) with*

columns forming a basis for $T_{\text{vec}(\bar{\Psi})}(\text{vec}(L^*))$. Here

$$\begin{aligned} T_{\text{vec}(\bar{\Psi})}(\text{vec}(L^*)) &= \text{vec}(T_{\bar{\Psi}}(L^*)) = \text{vec}(\nabla \Upsilon(\omega^*) T_{\Omega}(\omega^*)) \\ &= \{\text{vec}(\nabla_V \Upsilon(\omega^*) X + \nabla_B \Upsilon(\omega^*) Y + \nabla_C \Upsilon(\omega^*) Z + \nabla_{\gamma} \Upsilon(\omega^*) c) \mid \\ &\quad X \in R^{n \times d}, Y = \text{diag}(M), M \in R^{n \times n}, Z \in R^{d \times d}, c \in R\}. \end{aligned}$$

It can be shown that $T_{\bar{\Psi}}(L^*)$ is a linear subspace of $R^{n \times n}$ and $T_{\text{vec}(\bar{\Psi})}(\text{vec}(L^*))$ is a linear subspace of R^{n^2} .

Compared with Theorem 2, this theorem further requires that the matrix V is irreducible. The proof utilizes Theorem 4.4 in Geyer (1994), which provides the asymptotic distribution for a constrained M-estimator. The theoretical analysis is nontrivial, as it involves the manifold structure of our model parameters. Compared with Yu and Zhu (2025), we use more complicated tools to verify assumptions required for achieving the asymptotic normality. In particular, our asymptotic distribution involves a tangent cone with a special structure, and the non-symmetric kernel matrix in our model leads to a very different tangent cone that needs delicate derivations to arrive at its explicit form.

4 Simulations

In this section, we conduct simulation studies to examine the finite sample performance of our proposed method. As most existing work on hypergraphs, such as Yuan and Qu (2022) and Lyu et al. (2023), focus on uniform hyperedges, they are not directly comparable with our method. Correspondingly, we only include the model proposed by Yu and Zhu (2025) in our comparison. We will refer to Yu and Zhu (2025) as DPP and our proposed model as NDPP.

We simulate data from model (2) with parameters B, V, C, γ . For v_i 's, elements are independently generated from Uniform[0, 1], and then normalized to satisfy $\|v_i\| = 1$. We also consider a von Mise-Fisher (vMF) distribution, which is the spherical analogue of the normal distribution on the unit sphere. Its probability density function is given by $f(v) = C(\kappa) \exp(\kappa \mu^T v)$, where $C(\kappa)$ is the normalizing constant. When generating v_i 's from the vMF distribution, we set $\kappa = 10$ and $\mu = (1, 0, 0), (0, 1, 0)$ and $(0, 0, 1)$, so that the nodes belong to three clusters. For C , we first generate a matrix G with entries independently generated from Uniform[0, 1], set $C = G - G^T$ and then rescale C to ensure $\|C\|_F = 1$. The parameter γ is set as 0.15. For B , we generate $\eta_i \sim_{i.i.d.} \text{Beta}(1, 4)$ and set $\beta_i = 15s \cdot (0.2\eta_i + 0.05)$. This setting encourages only a small proportion of the nodes to have large popularity parameters. The parameter s is a scaling parameter that controls the sizes of hyperedges; see Figure 2. We let s vary from 1 to 7. The sampling algorithm is presented in Algorithm 1.

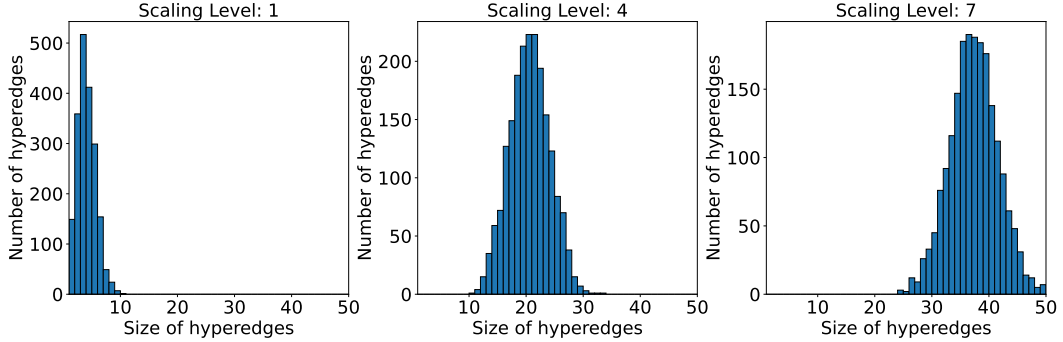


Figure 2: Histograms of hyperedge sizes under different scaling levels s when the number of nodes is $n = 100$ and the number of hyperedges is $m = 2000$.

To evaluate the estimation accuracy, we report relative estimation errors calculated as:

$$\frac{\min_{O \in O_d, S \in H_n} \|\hat{V} - SV^*O\|_F}{\|V^*\|_F}, \frac{\|\hat{G} - G^*\|_F}{\|G^*\|_F}, \frac{\|\hat{B} - B^*\|_2}{\|B^*\|_F}, \frac{\min_{S \in H_n} \|\hat{L} - SL^*S\|_F}{\|L^*\|_F},$$

where \hat{V} , \hat{G} , \hat{B} and \hat{L} are estimated parameters. Also reported is the relative estimation error of marginal and pairwise conditional edge probabilities, calculated as

$$\text{mean} \left(\left| \frac{\hat{P}_i - P_i^*}{P_i^*} \right| \right), \text{mean} \left(\left| \frac{\hat{P}_{j|i} - P_{j|i}^*}{P_{j|i}^*} \right| \right),$$

where $P_i = P(i \in E)$ and $P_{j|i} = P(j \in E \mid i \in E)$. Figures 3 and Figure S1 report the simulation results from 50 data replications under different distributions for V_i 's.

Figure 3 presents the log relative errors as the number of hyperedges m varies from 1000 to 4000 and the latent vector dimension d varies from 3 to 10. It is seen the estimated parameters and probabilities are close to the true values, and the estimation error decreases with m , consistent with our theoretical results. It can also be observed that the estimated marginal and conditional probabilities are not noticeably affected by d . Figure 4 shows how the relative errors vary with the scaling parameter s . It is seen that with a fixed m , the estimation error improves with the size of hyperedges.

Next, we compare the performance of DPP and NDPP models in two settings. In the first setting, the hyperedges are generated from the NDPP distribution, and in the second setting, the hyperedges are generated from the DPP distribution, using Algorithm 1 provided in [Kulesza et al. \(2012\)](#). In both settings, we estimate model parameter V , marginal probabilities and conditional probabilities using both the NDPP and DPP models. We set the number of nodes as $n = 100$, the dimension as $d = 3$, the scaling parameter as $s = 3$. The number of hyperedges m is set to vary from 100 to 4000.

Results from the first NDPP setting with uniformly distributed v_i 's are shown in Figures 5. It is seen that relative errors from the NDPP model decrease with m while the relative errors from the DPP

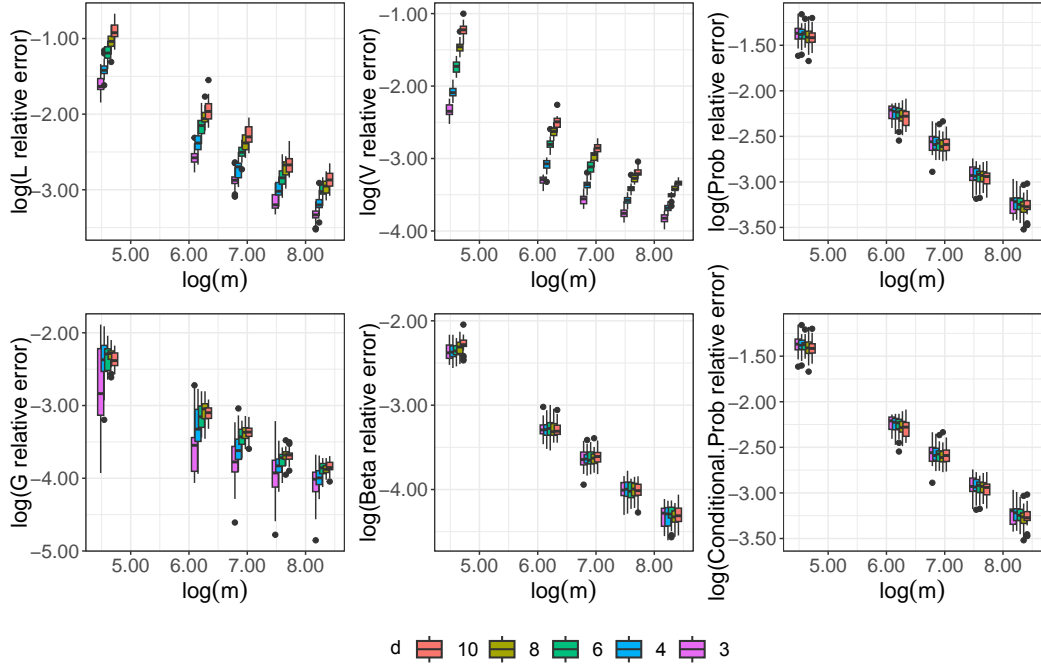


Figure 3: Relative errors under the NDPP model. Latent positions for nodes are uniformly generated with a variety dimensions d and a variety number of hyperedges m as $s = 3$ and $n = 100$.

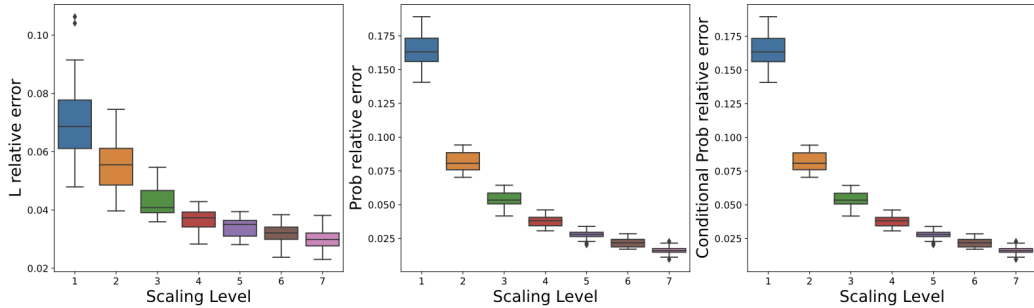


Figure 4: Relative errors under the NDPP model. Latent positions for nodes are uniformly generated with a variety scaling levels s as $d = 3, n = 100, m = 2000$.

model do not improve with m . Results from the second DPP setting with uniformly distributed for v_i 's are shown in Figures 6. Additional results with vMF distributed v_i 's are shown in the supplement. It is seen that relative errors from the NDPP and DPP model are comparable, and both decrease with m . This demonstrates that NDPP is a more flexible model and can be used in more general situations.

5 Real-world data examples

We apply the proposed NDPP model to four distinct hypergraphs, focusing on the task of hyperedge prediction. The first hypergraph, named *contact-high-school*, represents a human contact network constructed from interactions among high school students, recorded via wearable sensors. Here, the

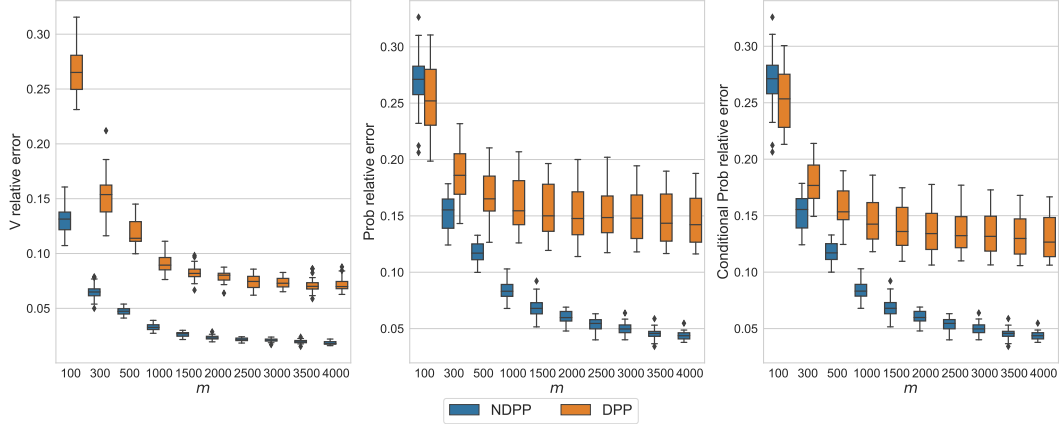


Figure 5: Comparison of relative errors under the NDPP and DPP model when the hyperedges are generated using NDPP. Latent positions for nodes are uniformly generated with a variety number of hypereges as $d = 3, s = 3, n = 100$.

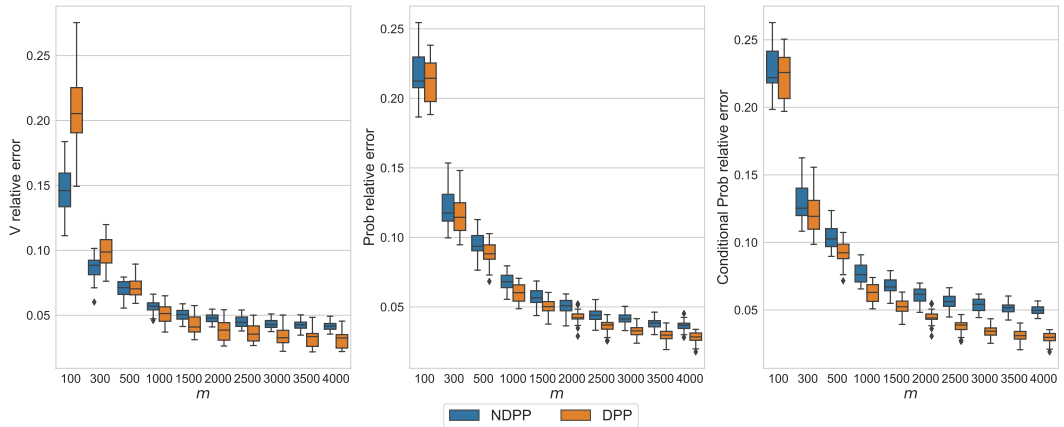


Figure 6: Comparison of relative errors under the NDPP and DPP model when the hyperedges are generated using DPP. Latent positions for nodes are uniformly generated with a variety number of hypereges as $d = 3, s = 3, n = 100$.

Data Set	Number of Nodes	Number of Hyperedges	Size of Hyperedges	
			Mean \pm Std	Range
contact-high-school	242	1535	2.051 ± 0.241	(2,4)
NDC-substances	343	10068	3.795 ± 3.039	(2,23)
tags-math-sx	302	15005	2.599 ± 0.802	(2,5)
email-Eu	153	25054	2.236 ± 1.139	(2,17)

Table 1: Summary of the four hypergraphs.

nodes are the students, and a hyperedge denotes the set of students recorded to be in close proximity to one another. The second hypergraph, named *email-Eu*, is an email network constructed from a European research institution. In this network, the nodes are email addresses, and a hyperedge represents the set of accounts involved in an email, including both the sender and all recipients. The third hypergraph, named *NDC-substances*, is a drug-related hypergraph constructed using data from the National Drug Code Directory. Nodes in this hypergraph correspond to individual substances (e.g., testosterone), and a hyperedge represents the collection of substances contained within a specific drug. The fourth hypergraph, named *tags-math-sx*, is a tag network derived from the Mathematics Stack Exchange forum. Here, the nodes are tags (annotations), and a hyperedge denotes the set of tags assigned to a question on the forum. Further details on these hypergraphs can be found in [Benson et al. \(2018\)](#). Table 1 provides a summary of these four hypergraphs.

On these four hypergraphs, we assess the performance of the DPP and NDPP models by evaluating their AUC (area under the ROC curve) and MPR (mean percentile rank) metrics. Hyperedges in each hypergraph are divided into training (80%) and test (20%) sets, and this procedure is repeated five times. The latent space dimension is fixed at 3 for the NDPP model. We also implemented NDPP and DPP by using the validation approach to select the latent space dimension. The results are consistent with our analyses, and are shown in Table S1 and Figure S3 in the supplement.

For AUC computation, we generate a set of random hyperedges matching sizes of true hyperedges in the test set, and calculate probabilities of both the randomly generated and true hyperedges using the fitted NDPP model. Labels are assigned as 1 for true hyperedges and 0 for the generated ones. The ROC curve then quantifies the model’s ability to distinguish between true hyperedges and randomly generated ones. An AUC of 1 indicates perfect discrimination, whereas an AUC of 0.5 implies no better than random guessing. For MPR evaluation, one node from each test hyperedge is randomly masked as missing, and the NDPP model predicts the missing node’s probability, conditional on the remaining nodes. The percentile rank of the true missing node is then calculated among all candidate nodes, and the MPR is derived by averaging these ranks across the test set. A percentile rank of 1 signifies the highest predictive accuracy, while a value of 0.5 indicates performance similar to random guessing.

Data Set	AUC		MPR	
	NDPP	DPP	NDPP	DPP
contact-high-school	0.720 \pm 0.015	0.680 \pm 0.009	0.724 \pm 0.009	0.690 \pm 0.007
NDC-substances	0.772 \pm 0.005	0.747 \pm 0.005	0.875 \pm 0.005	0.832 \pm 0.004
tags-math-sx	0.756 \pm 0.002	0.746 \pm 0.002	0.812 \pm 0.002	0.807 \pm 0.003
email-Eu	0.682 \pm 0.002	0.634 \pm 0.002	0.728 \pm 0.002	0.694 \pm 0.005

Table 2: Performance comparisons for the NDPP and DPP model

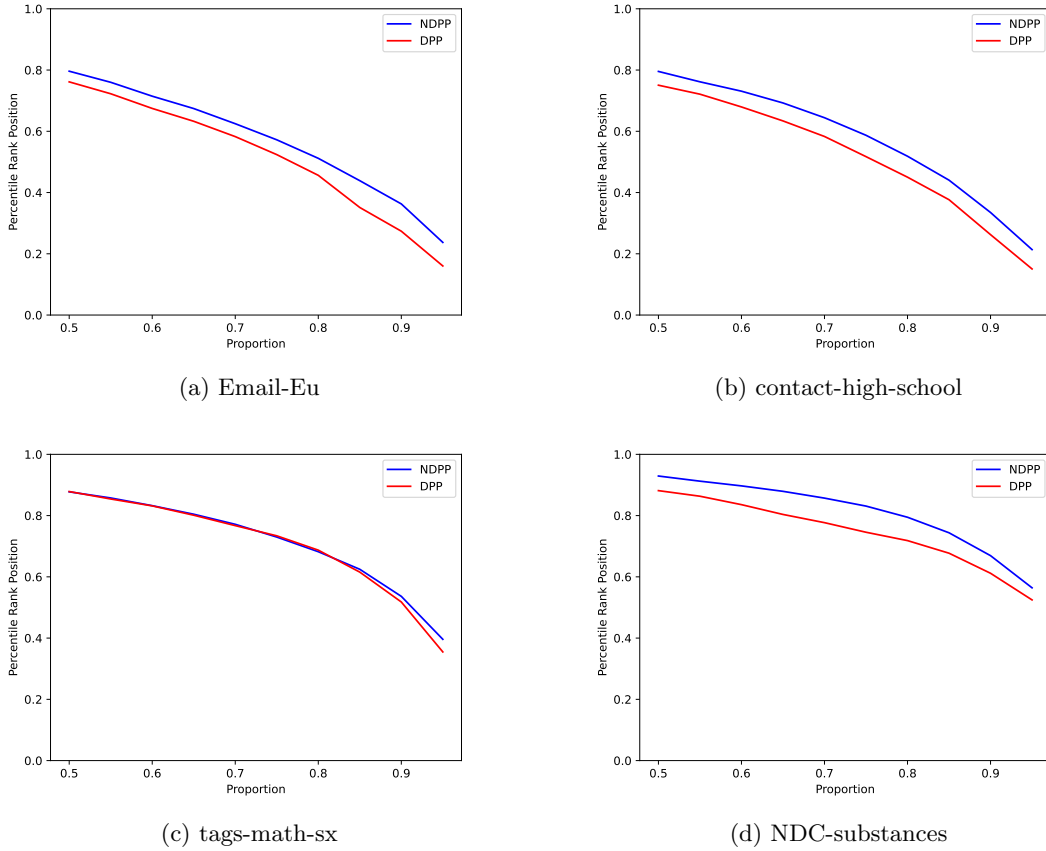


Figure 7: Proportion of nodes with varying percentile ranks.

Table 2 shows the AUC and MPR results from the DPP and NDPP models, respectively. We also display the curve of percentile rank based on all nodes in Figure 7. For three out of four datasets, including contact-high-school, NDC-substances and email-Eu, the NDPP model outperforms the DPP model. This aligns with the inherent characteristics of the models. In contact-high-school, NDC-substances and email-Eu, similar nodes may appear more frequently in hyperedges, and the DPP model’s node diversity assumption may not be appropriate. In contrary, in tags-math-sx, tags associated with a question tend to be more diverse. In this scenario, the DPP model performs similarly to the NDPP model.

6 Conclusion

In this paper, we propose a flexible model for non-uniform hypergraphs based on determinantal point processes, facilitating a significant reduction in the number of model parameters compared with tensor-based methods (Lyu et al., 2023). Our model is the first non-uniform hypergraph model that can encourage node similarity within hyperedges. The consistency and asymptotic normality of the MLE estimates of the model parameters are also established.

In the real-world data example part, we choose the dimension d using the validation approach. It is worth to investigate how to select d using a BIC-type criterion under our current framework. Additionally, extending the model to incorporate node-level covariates for more context-aware hyperedge formation is a worthwhile investigation. We leave these directions for future work.

References

Battiston, F., Amico, E., Barrat, A., Bianconi, G., Ferraz de Arruda, G., Franceschiello, B., Iacopini, I., Kéfi, S., Latora, V., Moreno, Y., et al. (2021). The physics of higher-order interactions in complex systems. *Nature Physics*, 17(10):1093–1098.

Benson, A. R., Abebe, R., Schaub, M. T., Jadbabaie, A., and Kleinberg, J. (2018). Simplicial closure and higher-order link prediction. *Proceedings of the National Academy of Sciences*, 115(48):E11221–E11230.

Bobrowski, O. and Kahle, M. (2018). Topology of random geometric complexes: a survey. *Journal of applied and Computational Topology*, 1:331–364.

Borcea, J., Brändén, P., and Liggett, T. (2009). Negative dependence and the geometry of polynomials. *Journal of the American Mathematical Society*, 22(2):521–567.

Brunel, V.-E. (2018). Learning signed determinantal point processes through the principal minor assignment problem. *Advances in Neural Information Processing Systems*, 31.

Cao, S., Lu, W., and Xu, Q. (2015). Grarep: Learning graph representations with global structural information. In *Proceedings of the 24th ACM international on conference on information and knowledge management*, pages 891–900.

Chien, I., Lin, C.-Y., and Wang, I.-H. (2018). Community detection in hypergraphs: Optimal statistical limit and efficient algorithms. In *International Conference on Artificial Intelligence and Statistics*, pages 871–879. PMLR.

Geyer, C. J. (1994). On the asymptotics of constrained m-estimation. *The Annals of statistics*, pages 1993–2010.

Ghoshdastidar, D. and Dukkipati, A. (2017a). Consistency of spectral hypergraph partitioning under planted partition model. *The Annals of Statistics*, 45(1).

Ghoshdastidar, D. and Dukkipati, A. (2017b). Uniform hypergraph partitioning: Provable tensor methods and sampling techniques. *Journal of Machine Learning Research*, 18(50):1–41.

Grover, A. and Leskovec, J. (2016). node2vec: Scalable feature learning for networks. In *Proceedings of the 22nd ACM SIGKDD international conference on Knowledge discovery and data mining*, pages 855–864.

Hoffmann, K. and Kunze, R. A. (1971). *Linear algebra*. Prentice-Hall New Jersey.

Kang, B. (2013). Fast determinantal point process sampling with application to clustering. *Advances in Neural Information Processing Systems*, 26.

Ke, Z. T., Shi, F., and Xia, D. (2019). Community detection for hypergraph networks via regularized tensor power iteration. *arXiv preprint arXiv:1909.06503*.

Kingma, D. P. and Ba, J. (2014). Adam: A method for stochastic optimization. In *International Conference on Learning Representations*.

Kulesza, A., Taskar, B., et al. (2012). Determinantal point processes for machine learning. *Foundations and Trends in Machine Learning*, 5(2–3):123–286.

Lavancier, F., Møller, J., and Rubak, E. (2015). Determinantal point process models and statistical inference. *Journal of the Royal Statistical Society Series B: Statistical Methodology*, 77(4):853–877.

Lunagómez, S., Mukherjee, S., Wolpert, R. L., and Airoldi, E. M. (2017). Geometric representations of random hypergraphs. *Journal of the American Statistical Association*, 112(517):363–383.

Lyu, Z., Xia, D., and Zhang, Y. (2023). Latent space model for higher-order networks and generalized tensor decomposition. *Journal of Computational and Graphical Statistics*, 32(4):1320–1336.

Nandy, S. and Bhattacharya, B. B. (2024). Degree heterogeneity in higher-order networks: Inference in the hypergraph β -model. *IEEE Transactions on Information Theory*, 70(8):6000–6024.

Poulson, J. (2020). High-performance sampling of generic determinantal point processes. *Philosophical Transactions of the Royal Society A*, 378(2166):20190059.

Qian, N. (1999). On the momentum term in gradient descent learning algorithms. *Neural networks*, 12(1):145–151.

Ritz, A., Tegge, A. N., Kim, H., Poirel, C. L., and Murali, T. (2014). Signaling hypergraphs. *Trends in biotechnology*, 32(7):356–362.

Tieleman, T. and Hinton, G. (2012). Lecture 6.5-rmsprop, coursera: Neural networks for machine learning. *University of Toronto, Technical Report*, 6.

Turnbull, K., Lunagómez, S., Nemeth, C., and Airoldi, E. (2023). Latent space modeling of hypergraph data. *Journal of the American Statistical Association*, pages 1–13.

Van der Vaart, A. W. (2000). *Asymptotic statistics*, volume 3. Cambridge university press.

Yu, S., Yang, H., Nakahara, H., Santos, G. S., Nikolić, D., and Plenz, D. (2011). Higher-order interactions characterized in cortical activity. *Journal of neuroscience*, 31(48):17514–17526.

Yu, X. and Zhu, J. (2025). Modeling hypergraphs with diversity and heterogeneous popularity. *Journal of the American Statistical Association*, (just-accepted):1–20.

Yuan, M., Liu, R., Feng, Y., and Shang, Z. (2022). Testing community structure for hypergraphs. *The Annals of Statistics*, 50(1):147–169.

Yuan, Y. and Qu, A. (2022). High-order joint embedding for multi-level link prediction. *Journal of the American Statistical Association*, 118(543).

Zhen, Y. and Wang, J. (2023). Community detection in general hypergraph via graph embedding. *Journal of the American Statistical Association*, 118(543):1620–1629.